Inorganic Chemistry

ARTICLE

pubs.acs.org/IC

Synthesis and Catalytic Properties of Molybdenum(VI) Complexes with Tris(3,5-dimethyl-1-pyrazolyl)methane

Patrícia Neves,[†] Sandra Gago,[†,‡] Salete S. Balula,[†,§] André D. Lopes,[∥] Anabela A. Valente,[*,†] Luís Cunha-Silva,[†,§] Filipe A. Almeida Paz,[†] Martyn Pillinger,[†] João Rocha,[†] Carlos M. Silva,[†] and Isabel S. Gonçalves[*,†]

[†]Department of Chemistry, CICECO, University of Aveiro, 3810-193 Aveiro, Portugal

[‡]Department of Chemistry, REQUIMTE, Faculty of Science and Technology, New University of Lisbon, 2829-516 Monte da Caparica, Portugal

[§]REQUIMTE/Department of Chemistry and Biochemistry, Faculty of Science, University of Porto, 4169-007 Porto, Portugal

[∥]Faculty of Science and Technology, Department of Chemistry, Biochemistry and Pharmacy, University of the Algarve, Campus de Gambelas, 8005-136 Faro, Portugal

Supporting Information

ABSTRACT: The complex $[MoO_2Cl\{HC(3,5\text{-}Me_2pz)_3\}]BF_4$ (**1**) ($HC(3,5\text{-}Me_2pz)_3$ = tris(3,5-dimethyl-1-pyrazolyl)methane) has been prepared and examined as a catalyst for epoxidation of olefins at 55 °C using *tert*-butyl hydroperoxide (TBHP) as the oxidant. For reaction of *cis*-cyclooctene, epoxycyclooctane is obtained quantitatively within 5 h when water is rigorously excluded from the reaction mixture. Increasing amounts of water in the reaction mixture lead to lower activities (without affecting product selectivity) and transformation of **1** into the trioxidomolybdenum(VI) complex $[\{HC(3,5\text{-}Me_2pz)_3\}MoO_3]$ (**4**). Complex **4** was isolated as a microcrystalline solid by refluxing a suspension of **1** in water. The powder X-ray diffraction pattern of **4** can be indexed in the orthorhombic *Pnma* system, with a = 16.7349(5) Å, b = 13.6380(4) Å, and c = 7.8513(3) Å. Treatment of **1** in dichloromethane with excess TBHP led to isolation of the symmetrical $[Mo_2O_4(\mu_2\text{-}O)\{HC(3,5\text{-}Me_2pz)_3\}_2](BF_4)_2$ (**2**) and unsymmetrical $[Mo_2O_3(O_2)_2(\mu_2\text{-}O)(H_2O)\{HC(3,5\text{-}Me_2pz)_3\}]$ (**3**) oxido-bridged dimers, which were characterized by single-crystal X-ray diffraction. Complex **2** displays the well-known $(Mo_2O_5)^{2+}$ bridging structure where each dioxidomolybdenum(VI) center is coordinated to three N atoms of the organic ligand and one μ_2-bridging O atom. The unusual complex **3** comprises dioxido and oxidodiperoxo molybdenum(VI) centers linked by a μ_2-bridging O atom, with the former center being coordinated to the tridentate N-ligand. The dinuclear complexes exhibit a similar catalytic performance to that found for mononuclear **1**. For complexes **1** and **2** use of the ionic liquids (ILs) 1-butyl-3-methylimidazolium tetrafluoroborate and *N*-butyl-3-methylpyridinium tetrafluoroborate as solvents allowed the complexes to be completely dissolved, and in each case the catalyst and IL could be recycled and reused without loss of activity.

INTRODUCTION

Scorpionate-type tris(pyrazolyl)methane (Tpm) ligands are the neutral analogues of the anionic tris(pyrazolyl)hydroborates (Tp).[1] They are formally derived from Tp by replacing the apical $\{BH\}^-$ anionic moiety with the isoelectronic CR group. Although metal complexes based on Tpm ligands were first reported in 1970,[2] they were much less studied than Tp systems mainly due to poor synthetic routes with low yields. Development of improved syntheses[3] has led to a renewed interest in this coordination chemistry, with applications in catalysis, photochemistry, and biomedicine.[1,4]

In his landmark paper on the coordination chemistry of poly(1-pyrazolyl)alkanes,[2] Trofimenko reported the reaction of $Mo(CO)_6$ with the ligands (L) tris(1-pyrazolyl)methane $[HC(pz)_3]$ and tris(3,5-dimethyl-1-pyrazolyl)methane $[HC(3,5\text{-}Me_2pz)_3]$ to give the tricarbonyl complexes $[Mo(CO)_3L]$. These complexes are useful starting materials for the preparation of other complexes in higher oxidation states. For example, complete oxidative decarbonylation with an excess of $SOCl_2$, I_2, Br_2, or HNO_3 leads to Mo^{III} (X = Cl, Br, I) or Mo^{VI} (X = O) complexes of the type $[MoX_3L]$.[5,6] Very recently, Pombeiro and co-workers reported that reaction of $Li[Mo(CO)_3(Tpms)]$ (Tpms = tris(1-pyrazolyl)methanesulfonate) with I_2 or HBF_4 affords the Tpms−Mo^{II} complexes $[Mo(CO)_3X(Tpms)]$ (X = I, H).[7] The latter are oxidized with air to give the dinuclear Mo^V complexes $[\{MoO(\mu_2\text{-}O)(Tpms)\}_2]$ and (in the presence of $CHCl_3$) $[\{MoOCl(Tpms)\}_2](\mu_2\text{-}O)$. Reaction of $Li[Mo(CO)_3(Tpms)]$ with $AgBF_4$ in air gave the dinuclear Mo^{VI} complex $[\{MoO_2(Tpms)\}_2](\mu_2\text{-}O)$. Enemark and co-workers also noted a tendency of Tpm−Mo mononuclear complexes to form dinuclear derivatives.[6] Reaction of the cationic monooxidomolybdenum(V) complex $[MoOCl_2\{HC(3,5\text{-}Me_2pz)_3\}]Cl$ with catechol in the presence of triethylamine initially gave a solution

Received: December 8, 2010
Published: March 25, 2011

Chart 1

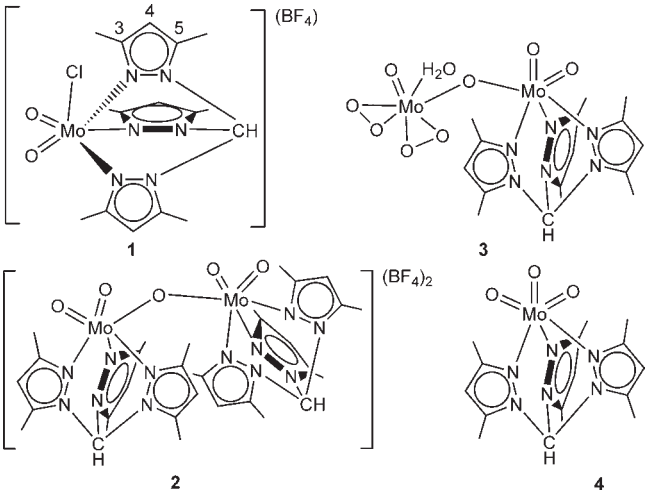

containing the mononuclear Mo^{V} complex $[MoOX_2\{HC(3,5\text{-}Me_2pz)_3\}]^-$ (X_2 = dianion of catechol), but upon standing of the reaction mixture the unsymmetrical dimer $[Mo_2O_4(OC_6H_4\text{-}O)\{HC(3,5\text{-}Me_2pz)_3\}]$ was isolated.

Reaction of $[MoO_2X_2(THF)_2]$ (X = Cl, Br) with $HC(pz)_3$ or $HC(3,5\text{-}Me_2pz)_3$ leads to replacement of both coordinated solvent molecules and one of the halo ligands to give $[MoO_2X(L)]X$.[8] These complexes are moderately active catalysts for the epoxidation of *cis*-cyclooctene with *tert*-butyl hydroperoxide (TBHP) as the oxidizing agent, giving 1,2-epoxycyclooctane as the only product. Santos et al. concluded that the organic ligand remained at least partially attached to the metal in the catalytically active center and determined its activity. We recently showed that the analogous complexes $[MoO_2Cl\{HC(bim)_3\}]X$ (X = Cl, BF_4, PF_6) containing the tridentate ligand tris(benzimidazolyl)methane exhibit a similar catalytic performance for olefin epoxidation.[9] The epoxide selectivity was very good with certain substrates, and the right combination of complex (X = Cl), ionic liquid (as solvent), and oxidant allowed efficient recovery of the catalyst/solvent mixture for use in subsequent reaction runs. When the complex $[MoO_2Cl\{HC(bim)_3\}]PF_6$ was used for the epoxidation of *cis*-cyclooctene with TBHP and no cosolvent, an insoluble solid recovered at the end of a catalytic run was tentatively identified as the dioxido(μ-oxido)molybdenum(VI) dimer $[Mo_2O_4(\mu_2\text{-}O)\{HC(bim)_3\}_2](Y)_2$ (Y = Cl, PF_6), which is analogous to the dinuclear Tpms−Mo^{VI} complex described in ref 7.

The studies outlined above suggested to us that more work needed to be done to understand the catalytic performance of complexes of the type $[MoO_2X(L)]X$ bearing Tpm ligands. In the present work the complex $[MoO_2Cl\{HC(3,5\text{-}Me_2pz)_3\}]BF_4$ (**1**) has been prepared and tested in catalytic olefin epoxidation. With the aim of obtaining a better understanding of the catalytically active species formed under the reactions conditions used, complex **1** was treated with excess TBHP, which resulted in the isolation of the symmetrical $[Mo_2O_4(\mu_2\text{-}O)\{HC(3,5\text{-}Me_2pz)_3\}_2](BF_4)_2$ (**2**) and unsymmetrical $[Mo_2O_3(O_2)_2(\mu_2\text{-}O)(H_2O)\{HC(3,5\text{-}Me_2pz)_3\}]$ (**3**) dimers. The single-crystal X-ray structures of **2** and **3** are described. The catalytic behaviors of all three complexes are compared, and the influence of water on formation of the different species is discussed.

RESULTS AND DISCUSSION

Synthesis. The complex $[MoO_2Cl\{HC(3,5\text{-}Me_2pz)_3\}]BF_4$ (**1**) was synthesized by addition of 1 equiv of the ligand $HC(3,5\text{-}Me_2pz)_3$ to a solution of $[MoO_2Cl(THF)_3](BF_4)$ in THF (Chart 1). Slow diffusion of diethyl ether into a concentrated solution of **1** in acetonitrile gave a small crop of single crystals suitable for X-ray diffraction. However, as described below, analysis of the data revealed a structure containing a symmetrical dioxido(μ-oxido)molybdenum(VI) complex, $[Mo_2O_4(\mu_2\text{-}O)\{HC(3,5\text{-}Me_2pz)_3\}_2](BF_4)_2$ (**2**), rather than the mononuclear dioxidomolybdenum(VI) complex; the presence of residual amounts of water in the system may have accounted for the conversion of a fraction of **1** into less soluble **2**. In an attempt to obtain a better understanding of the Mo species formed during catalytic olefin epoxidation with complex **1** as the catalyst precursor, reaction of **1** in CH_2Cl_2 with a large excess (ca. 150 equiv.) of the oxidant TBHP was performed separately. This gave a yellow solution from which the unsymmetrical dinuclear complex $[Mo_2O_3(O_2)_2(\mu_2\text{-}O)(H_2O)\{HC(3,5\text{-}Me_2pz)_3\}]$ (**3**) precipitated as a yellow solid upon stirring at room temperature. Crystals of **3** suitable for X-ray diffraction were obtained by recrystallization from 1,2-dichloroethane/diethyl ether/pentane. The CH_2Cl_2 filtrate obtained in the above procedure was treated with MnO_2 to destroy the excess peroxide. Addition of diethyl ether to the concentrated solution gave complex **2** (as confirmed by infrared and Raman spectroscopies and elemental analysis) as a colorless solid in 30% yield. Complex **1** may be transformed into **2** via hydrolysis of the Mo−Cl bonds and dimerization of the resultant metal species (the TBHP solution was used as received and may contain up to 4% water). Several dimers of the type $[Mo_2O_4(\mu_2\text{-}O)Cl_2(L)_n]$ (L = monodentate or bidentate ligand) have been obtained in an analogous fashion starting from monomers of the type $[MoO_2Cl_2(L)_{n/2}]$ in water or in water-containing systems and in the absence or in the presence of TBHP.[10] In an experiment to assess the stability of **1** toward moisture, a suspension of the complex in water was refluxed for 2 h. A white precipitate was obtained, which was identified (by infrared and Raman spectroscopies and elemental analysis) as being the trioxidomolybdenum(VI) complex $[\{HC(3,5\text{-}Me_2pz)_3\}MoO_3]$ (**4**), isolated in 51% yield. As reported previously,[6] complex **4** is insoluble in all common organic solvents. However, the solid obtained by the above procedure was microcrystalline, and its powder X-ray diffraction pattern could be indexed in the orthorhombic *Pnma* system, with a = 16.7349(5) Å, b = 13.6380(4) Å, and c = 7.8513(3) Å (see the Supporting Information for full details).

Infrared and Raman Spectroscopy. The infrared and Raman spectra of **1** in the solid state exhibit strong bands at 951 ± 1 and 917 ± 1 cm^{-1}, which are assigned to the symmetric and asymmetric Mo═O stretching vibrations, respectively, of the *cis*-$[MoO_2]^{2+}$ unit. Several intense bands between 1200 and 1600 cm^{-1} are assigned to internal ligand modes from the tridentate tris(3,5-dimethylpyrazolyl)methane ligand (e.g., the characteristic pyrazolyl ring stretching vibration at 1563 cm^{-1}), while a very strong and broad absorption centered at 1060 cm^{-1} is attributed to ν(B−F) of tetrafluoroborate anions. Complex **2** exhibits a very similar IR spectrum in the range of 900−1600 cm^{-1}, with the Mo═O stretching vibrations appearing at 916 and 945 cm^{-1} and ν(B−F) at about 1070 cm^{-1}. A medium-intensity band at 361 cm^{-1} in both the IR and the Raman spectra of **1** is assigned to a Mo−Cl stretching mode. As expected, this

dx.doi.org/10.1021/ic102456z |*Inorg. Chem.* 2011, 50, 3490–3500

Table 1. Bond Lengths (in Angstroms) for the Six Molybdenum Coordination Environments Present in $[Mo_2O_4(\mu_2\text{-}O)\{HC(3,5\text{-}Me_2pz)_3\}_2](BF_4)_2$ (2)

Mo(1)−O(1)	1.683(5)	Mo(4)−O(6)	1.888(5)
Mo(1)−O(2)	1.664(6)	Mo(4)−O(9)	1.696(5)
Mo(1)−O(3)	1.892(5)	Mo(4)−O(10)	1.689(6)
Mo(1)−N(1)	2.296(7)	Mo(4)−N(19)	2.291(6)
Mo(1)−N(3)	2.231(6)	Mo(4)−N(21)	2.234(6)
Mo(1)−N(5)	2.304(6)	Mo(4)−N(35)	2.290(6)
Mo(2)−O(3)	1.886(5)	Mo(5)−O(11)	1.890(5)
Mo(2)−O(4)	1.690(6)	Mo(5)−O(12)	1.709(5)
Mo(2)−O(5)	1.693(5)	Mo(5)−O(13)	1.691(5)
Mo(2)−N(7)	2.314(6)	Mo(5)−N(25)	2.213(6)
Mo(2)−N(9)	2.204(6)	Mo(5)−N(27)	2.319(7)
Mo(2)−N(11)	2.325(7)	Mo(5)−N(29)	2.308(7)
Mo(3)−O(6)	1.896(5)	Mo(6)−O(11)	1.887(5)
Mo(3)−O(7)	1.683(6)	Mo(6)−O(14)	1.698(5)
Mo(3)−O(8)	1.688(5)	Mo(6)−O(15)	1.680(5)
Mo(3)−N(13)	2.219(6)	Mo(6)−N(31)	2.314(7)
Mo(3)−N(15)	2.289(7)	Mo(6)−N(33)	2.310(6)
Mo(3)−N(17)	2.289(6)	Mo(6)−N(35)	2.230(6)

band is absent for **2**. Complex **1** exhibits a medium-intensity band at 762 cm^{-1} in the IR spectrum, which is assigned to a ligand mode. The corresponding band in the spectrum of **2** appears with much higher intensity, which is attributed to overlap of the ligand mode with a ν(Mo−O−Mo) vibration. This latter assignment is fully consistent with literature data for other examples of dioxido-(μ-oxido)molybdenum(VI) dimers, which typically exhibit the ν(Mo−O−Mo) mode as a strong band in the 750−800 cm^{-1} region of the IR spectrum.[7,10] For complex **3** two well-separated and strong bands are observed at 760 and 794 cm^{-1} in the IR spectrum; the former band is assigned to a ligand mode, while the latter is assigned to ν(Mo−O−Mo). The *cis*-$[MoO_2]^{2+}$ fragment in **3** gives rise to two strong Mo═O stretching vibrations at 915 and 954 cm^{-1} in the IR spectrum (920 and 948 cm^{-1} in the Raman), in agreement with that observed for complex **1**. In addition, the bands at 985 [strong in the Raman (not observed for **1**), weaker in the IR], 862 (medium in the IR), and 567 (medium in the IR) are assigned to ν(Mo═O), ν(O−O), and ν[Mo−O(O_2)], respectively, from the oxidodiperoxo fragment. The IR spectrum of **3** contains no band for ν(B−F), which is consistent with the complex being neutral. Complex **4** exhibits three ν(Mo═O) absorptions at 899, 861, and 840 cm^{-1}, in agreement with that reported by Enemark and co-workers for the same complex, which was prepared in 40% yield by exhaustive oxidation of $[\{HC(3,5\text{-}Me_2pz)_3\}Mo(CO)_3]$ with nitric acid.[6]

Crystal Structure Descriptions. The single crystals obtained as described above were analyzed by X-ray diffraction, allowing a full crystallographic description. The two crystal structures are formulated as $[Mo_2O_4(\mu_2\text{-}O)\{HC(3,5\text{-}Me_2pz)_3\}_2](BF_4)_2$ (**2**) and $[Mo_2O_3(O_2)_2(\mu_2\text{-}O)(H_2O)\{HC(3,5\text{-}Me_2pz)_3\}]\cdot 3H_2O$ (**3**). Complex **2** crystallizes in the triclinic space group $P\bar{1}$ having three crystallographically independent cationic $[Mo_2O_4(\mu_2\text{-}O)\{HC(3,5\text{-}Me_2pz)_3\}_2]^{2+}$ units and six BF_4^- anions composing the asymmetric unit (asu), whereas complex **3** crystallizes in the monoclinic space group $P2_1/c$ with a neutral complex $[Mo_2O_3(O_2)_2(\mu_2\text{-}O)(H_2O)\{HC(3,5\text{-}Me_2pz)_3\}]$ and three water molecules of crystallization comprising the asu (Figure S2 in the Supporting Information). Due to the similar features of the three crystallographically independent complex units in **2**, the structural discussion will be mainly focused on the cationic complex which is formed by Mo(1) and Mo(2). Unless otherwise stated, these assumptions are valid for the remaining crystallographically independent complexes. Selected bond lengths and angles for the six molybdenum coordination environments present in **2** are listed in Tables 1 and 2.

Table 2. Bond Angles (in degrees) for the Six Molybdenum Coordination Environments Present in $[Mo_2O_4(\mu_2\text{-}O)\{HC(3,5\text{-}Me_2pz)_3\}_2](BF_4)_2$ (2)

O(1)−Mo(1)−O(3)	103.3(2)	O(6)−Mo(3)−N(13)	160.4(2)
O(1)−Mo(1)−N(1)	160.8(2)	O(6)−Mo(3)−N(15)	89.8(2)
O(1)−Mo(1)−N(3)	89.9(2)	O(6)−Mo(3)−N(17)	87.9(2)
O(1)−Mo(1)−N(5)	85.7(2)	O(7)−Mo(3)−O(6)	103.5(2)
O(2)−Mo(1)−O(1)	104.3(3)	O(7)−Mo(3)−O(8)	103.0(3)
O(2)−Mo(1)−O(3)	103.7(3)	O(7)−Mo(3)−N(13)	88.8(2)
O(2)−Mo(1)−N(1)	89.5(3)	O(7)−Mo(3)−N(15)	159.9(2)
O(2)−Mo(1)−N(3)	91.1(3)	O(7)−Mo(3)−N(17)	88.8(3)
O(2)−Mo(1)−N(5)	163.2(3)	O(8)−Mo(3)−O(6)	102.7(2)
O(3)−Mo(1)−N(1)	85.8(2)	O(8)−Mo(3)−N(13)	88.9(2)
O(3)−Mo(1)−N(3)	156.8(2)	O(8)−Mo(3)−N(15)	88.2(3)
O(3)−Mo(1)−N(5)	86.7(2)	O(8)−Mo(3)−N(17)	161.6(2)
N(1)−Mo(1)−N(5)	78.0(2)	N(13)−Mo(3)−N(15)	74.6(2)
N(3)−Mo(1)−N(1)	76.4(2)	N(13)−Mo(3)−N(17)	77.1(2)
N(3)−Mo(1)−N(5)	75.2(2)	N(15)−Mo(3)−N(17)	76.6(2)
O(3)−Mo(2)−N(7)	89.1(2)	O(6)−Mo(4)−N(19)	88.2(2)
O(3)−Mo(2)−N(9)	157.2(2)	O(6)−Mo(4)−N(21)	160.6(2)
O(3)−Mo(2)−N(11)	85.1(2)	O(6)−Mo(4)−N(23)	90.2(2)
O(4)−Mo(2)−O(3)	103.3(2)	O(9)−Mo(4)−O(6)	102.4(3)
O(4)−Mo(2)−O(5)	104.1(3)	O(9)−Mo(4)−N(19)	161.2(2)
O(4)−Mo(2)−N(7)	86.8(3)	O(9)−Mo(4)−N(21)	89.8(3)
O(4)−Mo(2)−N(9)	91.5(2)	O(9)−Mo(4)−N(23)	87.3(3)
O(4)−Mo(2)−N(11)	162.3(2)	O(10)−Mo(4)−O(6)	102.4(2)
O(5)−Mo(2)−O(3)	102.8(3)	O(10)−Mo(4)−O(9)	104.6(3)
O(5)−Mo(2)−N(7)	161.3(2)	O(10)−Mo(4)−N(19)	87.9(3)
O(5)−Mo(2)−N(9)	89.9(2)	O(10)−Mo(4)−N(21)	88.7(3)
O(5)−Mo(2)−N(11)	88.8(3)	O(10)−Mo(4)−N(23)	160.1(2)
N(7)−Mo(2)−N(11)	77.7(2)	N(21)−Mo(4)−N(19)	76.3(2)
N(9)−Mo(2)−N(7)	74.4(2)	N(21)−Mo(4)−N(23)	75.3(2)
N(9)−Mo(2)−N(11)	76.3(2)	N(23)−Mo(4)−N(19)	77.0(2)
O(11)−Mo(5)−N(25)	157.5(2)	O(11)−Mo(6)−N(31)	87.7(2)
O(11)−Mo(5)−N(27)	87.2(2)	O(11)−Mo(6)−N(33)	85.5(2)
O(11)−Mo(5)−N(29)	85.7(2)	O(11)−Mo(6)−N(35)	157.2(2)
O(12)−Mo(5)−O(11)	103.1(2)	O(14)−Mo(6)−O(11)	103.2(2)
O(12)−Mo(5)−N(25)	90.2(2)	O(14)−Mo(6)−N(31)	162.3(3)
O(12)−Mo(5)−N(27)	85.7(3)	O(14)−Mo(6)−N(33)	89.4(3)
O(12)−Mo(5)−N(29)	160.7(2)	O(14)−Mo(6)−N(35)	89.9(3)
O(13)−Mo(5)−O(11)	103.1(2)	O(15)−Mo(6)−O(11)	103.6(2)
O(13)−Mo(5)−O(12)	104.5(3)	O(15)−Mo(6)−O(14)	103.5(3)
O(13)−Mo(5)−N(25)	90.7(3)	O(15)−Mo(6)−N(31)	87.2(3)
O(13)−Mo(5)−N(27)	163.1(2)	O(15)−Mo(6)−N(33)	161.8(3)
O(13)−Mo(5)−N(29)	89.8(3)	O(15)−Mo(6)−N(35)	91.1(2)
N(25)−Mo(5)−N(27)	75.6(2)	N(33)−Mo(6)−N(31)	77.4(2)
N(25)−Mo(5)−N(29)	76.5(2)	N(35)−Mo(6)−N(31)	75.5(2)
N(29)−Mo(5)−N(27)	77.5(2)	N(35)−Mo(6)−N(33)	75.9(2)

dx.doi.org/10.1021/ic102456z |*Inorg. Chem.* 2011, 50, 3490–3500

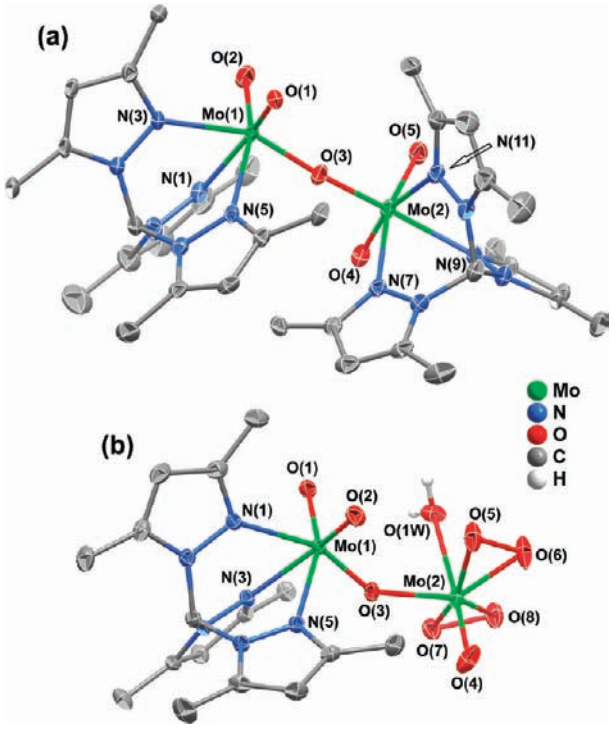

Figure 1. Schematic representation of the (a) $[Mo_2O_4(\mu_2\text{-}O)\{HC(3,5\text{-}Me_2pz)_3\}_2]^{2+}$ and (b) $[Mo_2O_3(O_2)_2(\mu_2\text{-}O)(H_2O)\{HC(3,5\text{-}Me_2pz)_3\}]$ dinuclear complexes present in compounds **2** and **3**, respectively. The labeling scheme for all atoms composing the molybdenum coordination environments is provided. Thermal ellipsoids are drawn at the 50% probability level, and for clarity, all H atoms bonded to carbon have been omitted. For details on the represented bond lengths and angles, see Tables 1−3.

Table 3. Selected Bond Lengths (in Angstroms) and Angles (in degrees) for the Molybdenum Coordination Environments Present in $[Mo_2O(O_2)_2(\mu_2\text{-}O)(H_2O)\{HC(3,5\text{-}Me_2pz)_3\}]\cdot 3H_2O$ (3)

{Mo(1)N_3O_3}		{Mo(2)O_7}	
Mo(1)−O(1)	1.6986(15)	Mo(2)−O(3)	2.0259(14)
Mo(1)−O(2)	1.7213(15)	Mo(2)−O(4)	1.6785(18)
Mo(1)−O(3)	1.8098(14)	Mo(2)−O(5)	1.9589(17)
Mo(1)−N(1)	2.2865(17)	Mo(2)−O(6)	1.9408(17)
Mo(1)−N(3)	2.3289(17)	Mo(2)−O(7)	1.9538(16)
Mo(1)−N(5)	2.3363(17)	Mo(2)−O(8)	1.9345(16)
		Mo(2)−O(1W)	2.3152(17)
		O(5)−O(6)	1.477(2)
		O(7)−O(8)	1.476(2)
O(1)−Mo(1)−O(2)	103.77(7)	O(3)−Mo(2)−O(4)	94.54(7)
O(1)−Mo(1)−O(3)	105.10(7)	O(3)−Mo(2)−O(5)	87.13(6)
O(1)−Mo(1)−N(1)	88.58(7)	O(3)−Mo(2)−O(6)	131.31(7)
O(1)−Mo(1)−N(3)	158.91(7)	O(3)−Mo(2)−O(7)	89.45(6)
O(1)−Mo(1)−N(5)	87.82(7)	O(3)−Mo(2)−O(8)	133.34(7)
O(2)−Mo(1)−O(3)	104.69(7)	O(3)−Mo(2)−O(1W)	82.18(6)
O(2)−Mo(1)−N(1)	88.58(7)	O(4)−Mo(2)−O(5)	102.25(9)
O(2)−Mo(1)−N(3)	88.93(6)	O(4)−Mo(2)−O(6)	100.40(9)
O(2)−Mo(1)−N(5)	158.59(6)	O(4)−Mo(2)−O(7)	101.45(8)
O(3)−Mo(1)−N(1)	158.36(7)	O(4)−Mo(2)−O(8)	101.44(8)
O(3)−Mo(1)−N(3)	87.42(6)	O(4)−Mo(2)−O(1W)	176.71(7)
O(3)−Mo(1)−N(5)	89.17(6)	O(5)−Mo(2)−O(6)	44.52(7)
N(1)−Mo(1)−N(3)	74.97(6)	O(5)−Mo(2)−O(7)	156.24(8)
N(1)−Mo(1)−N(5)	74.42(6)	O(5)−Mo(2)−O(8)	130.33(7)
N(3)−Mo(1)−N(5)	75.24(6)	O(5)−Mo(2)−O(1W)	77.70(7)
		O(6)−Mo(2)−O(7)	131.28(7)
		O(6)−Mo(2)−O(8)	88.54(7)
		O(6)−Mo(2)−O(1W)	81.90(8)
		O(7)−Mo(2)−O(8)	44.62(7)
		O(7)−Mo(2)−O(1W)	78.54(7)
		O(8)−Mo(2)−O(1W)	80.90(7)

The molecular structures of the cationic and neutral dinuclear complexes are depicted in Figure 1. In both complexes the Mo^{VI} centers are bridged by an oxygen atom (μ_2-bridging oxido group), imposing Mo···Mo distances of 3.7666(1), 3.7702(1), and 3.7707(1) Å [average of 3.691(1) Å] and Mo−O−Mo angles of 170.118(3)°, 171.347(4)°, and 173.064(3)° [average of 171.510(4)°] for the three crystallographically independent complex residues in **2** and a Mo(1)···Mo(2) distance of 3.6513(1) Å and Mo(1)−O(3)−Mo(2) angle of 144.264(3)° in **3**. The shorter intermetallic distance in **3** is attributed to the features of the coordination environment of the Mo(2) center which is less sterically hindered. The two Mo^{VI} centers in $[Mo_2O_4(\mu_2\text{-}O)\{HC(3,5\text{-}Me_2pz)_3\}_2]^{2+}$ have identical distorted octahedral coordination environments, {MoN_3O_3}, being connected to three N atoms of one $HC(3,5\text{-}Me_2pz)_3$ ligand, two terminal oxido groups, and a μ_2-bridging oxido group (Figure 1a). The high degree of distortion observed in the octahedral geometries is confirmed by the bond distances and internal octahedral angles: as expected, for all crystallographically independent moieties, the Mo═O distances range between 1.664(6) and 1.709(5) Å and are markedly shorter than the Mo−O−Mo distances of the μ_2-O bridges which are instead found in the 1.886(5)−1.896(5) Å range. Additionally, the lengths of the trans Mo−N bonds with respect to the terminal Mo═O bonds [from 2.289(6) to 2.325(7) Å] are greater than those which are trans to the μ_2-O bridges [2.213(6)−2.234(6) Å], which is probably a direct consequence of the well-known trans effect of Mo═O. The cis and trans internal octahedral (N,O)−Mo−(N,O) angles are found in the 74.4(2)−104.6(3)° and 156.8(2)−163.2(3)° ranges, respectively (Table 2), considerably spreading around the expected values for ideal octahedral environments.

In the asymmetrical dinuclear complex $[Mo_2O_3(O_2)_2(\mu_2\text{-}O)(H_2O)\{HC(3,5\text{-}Me_2pz)_3\}]$, Mo(1) has a similar environment to that described for **2**, being coordinated to three N atoms of the organic ligand, two terminal O atoms, and a μ_2-bridging O atom (Figure 1b), exhibiting a highly distorted octahedral coordination environment with the Mo(1)−O,N bond lengths and (N,O)−Mo−(N,O) angles being comparable to those of **2** (Table 3). The Mo(2) center in **3** is absolutely distinct, coordinating to one oxido group, two peroxo moieties, one water molecule, and a μ_2-bridging oxido group, in an overall hepta-coordination environment, {MoO_7}, which geometrically resembles a distorted pentagonal bipyramid, for which the equatorial plane is composed of the four O atoms from the two peroxo groups [O(5), O(6), O(7), and O(8)], with Mo(2)−O distances in the 1.9345(16)−1.9589(17) Å range, and by the μ_2-bridging O atom, with an Mo(2)−O(3) distance of 2.0259(14) Å (Table 3 and Figure 1b). This center is displaced by ca. 0.33 Å from the equatorial plane [defined by O(3), O(5), O(6), O(7), and O(8)] in the direction of the apical O(4) oxido group. The axial positions of the pentagonal bipyramid are occupied by the latter group and by the O atom of the coordinated water molecule, with the bond distance being 2.3152(17) Å (Table 3 and Figure 1b). The cis and trans O−Mo(2)−O angles are found in the 44.52(7)−102.25(9)° and 131.28(7)−176.71(7)°

dx.doi.org/10.1021/ic102456z |*Inorg. Chem.* 2011, 50, 3490–3500

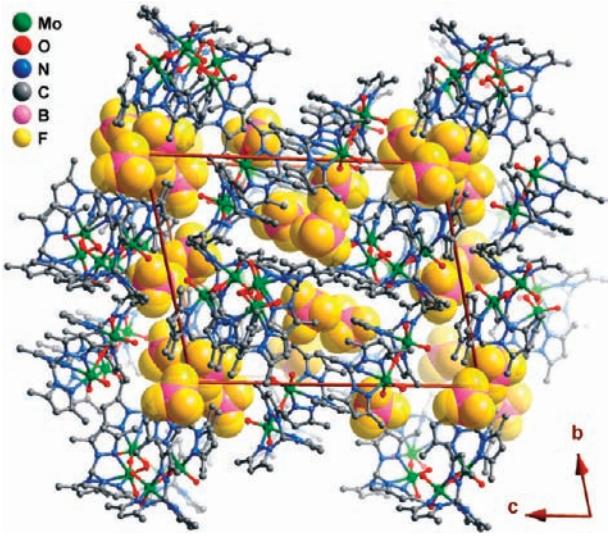

Figure 2. Mixed ball-and-stick (cationic complexes) and space-filling (BF_4^- anions) representation of the crystal packing of $[Mo_2O_4(\mu_2\text{-}O)\{HC(3,5\text{-}Me_2pz)_3\}_2](BF_4)_2$ (**2**), viewed in perspective along the [100] crystallographic direction. All H atoms have been omitted for clarity.

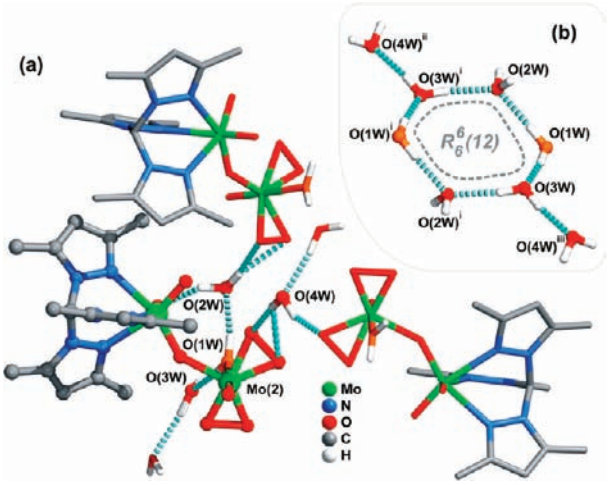

Figure 3. Schematic representation of the hydrogen bonds (light-blue dashed lines) found in $[Mo_2O_3(O_2)_2(\mu_2\text{-}O)(H_2O)\{HC(3,5\text{-}Me_2pz)_3\}]\cdot 3H_2O$ (**3**): (a) hydrogen-bonding interactions involving all water molecules and interconnecting neighboring complexes (atoms of the asymmetric unit are represented in ball-and-stick mode); (b) $(H_2O)_8$ cluster, where the O atoms shown as red and orange represent the uncoordinated and coordinated water molecules, respectively [symmetry transformations used to generate equivalent atoms: (i) $-x, -y+1, -z+1$; (ii) $-x, y+1/2, -z+1/2$; (iii) $x, -y+1/2, z+1/2$]. For clarity, only the H atoms associated with the water molecules are represented. Table 4 collects all relevant details on the hydrogen-bonding geometries.

ranges. The wider ranges for these angles arise from the presence of the peroxo groups which contribute, at each coordinating position, two oxygen donor atoms. The geometric features of the Mo(2) center, including bond distances and angles, are comparable to those reported for related dinuclear Mo complexes.[11]

The crystal packing of dinuclear $[Mo_2O_4(\mu_2\text{-}O)\{HC(3,5\text{-}Me_2pz)_3\}_2]^{2+}$ cationic complexes in **2**, mediated by C−H···O weak hydrogen bonds (not shown; C···O distances found between ca. 3.07 and 3.19 Å), leads to voids which are occupied by the BF_4^- counterions (Figure 2 and Figure S3 in the Supporting Information). The crystal packing further induces the presence of a number of weak C−H···F contacts connecting the cationic complexes to BF_4^- (not shown); all C···F distances are in the 2.925−3.169 Å range.

Table 4. Hydrogen-Bonding Geometries (distances in Angstroms and angles in degrees) for $[Mo_2O(O_2)_2(\mu_2\text{-}O)(H_2O)\{HC(3,5\text{-}Me_2pz)_3\}]\cdot 3H_2O$ (3)[a]

D−H···A	d(D···A)	<(DHA)
O(1W)−H(1W)···O(2W)	2.812(2)	168(2)
O(1W)−H(2W)···O(3W)	2.712(3)	172(2)
O(2W)−H(3W)···O(7)[i]	2.862(2)	172(2)
O(2W)−H(3W)···O(8)[i]	2.996(2)	145(2)
O(2W)−H(4W)···O(2)	2.778(2)	152(3)
O(3W)−H(5W)···O(2W)[ii]	2.881(3)	173(3)
O(3W)−H(6W)···O(4W)[iii]	2.854(3)	171(3)
O(4W)−H(7W)···O(5)	2.856(3)	171(3)
O(4W)−H(7W)···O(6)	3.435(3)	142(2)
O(4W)−H(8W)···O(6)[iv]	2.976(3)	149(2)

[a] Symmetry transformations used to generate equivalent atoms: (i) $x, -y+1/2, z-1/2$; (ii) $-x, -y+1, -z+1$; (iii) $x, -y+1/2, z+1/2$; (iv) $-x, -y, -z+1$.

Water molecules play a decisive role in the crystal packing of compound **3**. Indeed, as depicted in Figure 3a, the O atoms of the peroxo groups [O(5), O(6), O(7), and O(8)] and the coordinated water molecule [O1(W)] composing the coordination sphere of Mo(2) are engaged in a series of strong and highly directional O−H···O hydrogen-bonding interactions with the uncoordinated water molecules [O2(W), O3(W), and O4(W)] (Figure 3a and Table 4). These are engaged in cooperative water-to-water interactions [O(3W)−H(5W)···O(2W)[ii] and O(3W)−H(6W)···O(4W)[iii]; Figure 3b and Table 4] and form angular clusters of the type $(H_2O)_3$. Two neighboring water clusters interact with the coordinated water molecules to originate a cyclic cluster comprising eight water moieties, $(H_2O)_8$, which can be systematically represented by the graph set motif $R_6^6(12)$. Recently, various reports have described distinct types of discrete water clusters such as tetramers,[13] hexamers,[14] octamers,[15] decamers,[16] dodecamers,[17] and other larger agglomerates.[18] A number of polymeric water clusters, mainly chains (1D clusters),[19] some layers (2D clusters),[20] and a handful of frameworks (3D clusters),[21] are also described in the literature.[22]

A remarkable feature of compound **3** concerns the fact that the O−H···O hydrogen-bonding interactions connecting each individual complex to the water molecules of crystallization led to formation of a 2D hydrogen-bonded network as shown in Figure 4a. Layers are built up by parallel rows of individual $[Mo_2O_3(O_2)_2(\mu_2\text{-}O)(H_2O)\{HC(3,5\text{-}Me_2pz)_3\}]$ complexes (pointing in opposite directions) and interconnected by the water molecules of crystallization. Individual layers close pack along the [100] direction of the unit cell (Figure 4b) with the structural cohesion of this packing being reinforced by the presence of a number of cooperative weak C−H···O hydrogen bonds (not shown) involving the CH groups of one layer and the O atoms (from the oxido and peroxo groups and water molecules) of the adjacent one.

Catalytic Tests. The catalytic performance of $[MoO_2Cl\{HC(3,5\text{-}Me_2pz)_3\}]BF_4$ (**1**) was investigated in the reaction of *cis*-cyclooctene

dx.doi.org/10.1021/ic102456z |*Inorg. Chem.* 2011, 50, 3490–3500

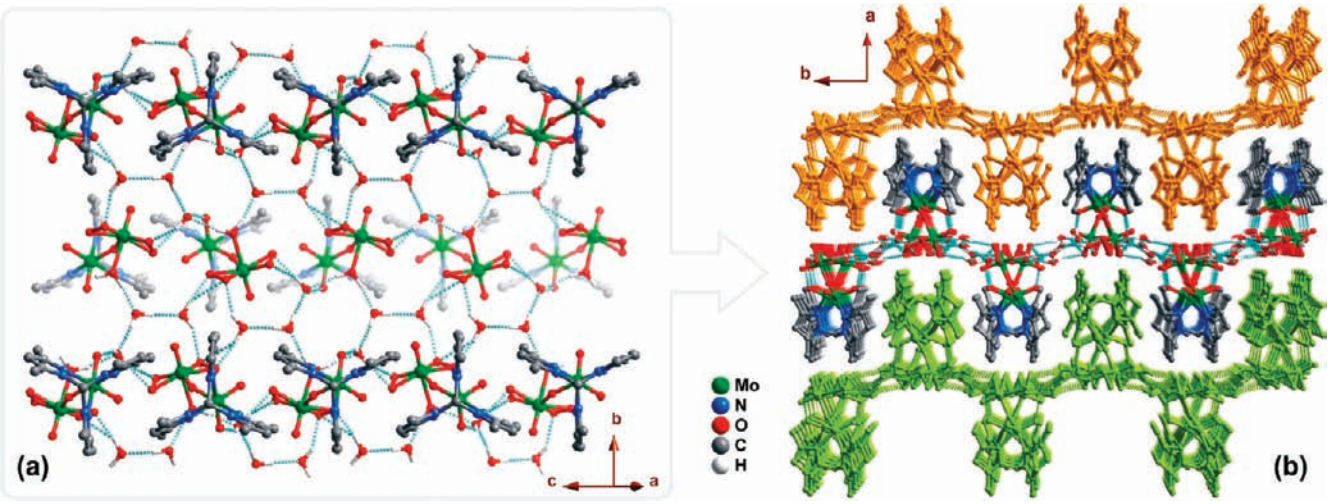

Figure 4. Ball-and-stick representation of the 2D hydrogen-bonded networks (infinite layers) involving the $[Mo_2O_3(O_2)_2(\mu_2\text{-}O)(H_2O)\{HC(3,5\text{-}Me_2pz)_3\}]$ complexes and the water molecules of crystallization: (a) single layer with the complexes of adjacent rows pointing above and below the plane of the layer; (b) perspective view along the [001] direction of the unit cell showing the packing of layers, with neighboring nets represented in different colors. Hydrogen bonds are represented as dashed lines, and for clarity, only the H atoms of water molecules are shown.

(Cy) with *tert*-butyl hydroperoxide (5−6 M in decane, denoted TBHPorg) at 55 °C using a Mo:olefin:oxidant molar ratio of 0.01:1.0:1.7. Complex **1** is not completely soluble under the reaction conditions used, originating a yellow opaque mixture. Epoxycyclooctane (CyO) was obtained as the only product in 97% yield at 24 h reaction (Table 5 and Figure 5). Blank tests indicated that the reaction did not take place to a significant extent in the absence of complex (4% Cy conversion at 24 h), in the absence of oxidant (0%), or when the ligand $HC(3,5\text{-}Me_2pz)_3$ was used instead of the Mo^{VI} complex (3%). Hence, the simultaneous presence of the molybdenum species and the oxidant was required for the catalytic epoxidation to take place. On the basis of the CyO yield at 24 h these results are at least as good if not better than those reported in the literature for other ionic complexes that differ from **1** in the counterion or in the tridentate organic Lewis base ligand used as catalysts in the same reaction under similar conditions: $[MoO_2Cl\{HC(3,5\text{-}Me_2pz)_3\}]Cl$ gave ca. 75%,[8] $[MoO_2Cl(Bn_3Me_3\text{-tame})]BF_4$ gave 45% (Bn_3Me_3-tame = *N*,*N*′,*N*″-tribenzyl-1,1,1-tris(methylaminomethyl)ethane),[23] and $[MoO_2Cl\{HC(bim)_3\}]BF_4$ gave ca. 93% ($HC(bim)_3$ = tris(benzimidazolyl)methane).[9]

As indicated above, the reaction mixture after 24 h consisted of a solid suspended in a yellow liquid. The solid and liquid phases were separated as described in the Experimental Section, and the recovered beige solid (hereafter referred to as **1**-TBHPorg) was used in a second reaction run of 24 h. The kinetic curves were essentially identical for the two runs, as were the CyO yields at 6 and 24 h (Figure 5 and Table 5). GC-MS analysis of the liquid phase from the first run revealed the presence of free $HC(3,5\text{-}Me_2pz)_3$. The ATR FT-IR spectrum of **1**-TBHPorg exhibited some differences in the ranges of 800−1150 and 300−400 cm^{-1} when compared with complex **1**, suggesting that the complex was not completely stable under the reaction conditions used (Figure S5 in the Supporting Information). As will be discussed below, these changes can be attributed to the water sensitivity of **1** (the TBHP was used as received and may contain up to 4% water, which means that the H_2O:Mo molar ratio could be as high as 50:1 under the reaction conditions used) and its transformation into other species, namely, complex **4** and possibly also complexes **2** and **3**. Accordingly, when the catalytic run was repeated but with water removed from the Cy/TBHPorg system (by using molecular sieves) prior to addition of **1** and heating to 55 °C (experiment denoted as **1**/Cy/dryTBHPorg) not only was an increase in the reaction rate observed (61%/100% CyO yield at 10 min/5 h compared with 23%/86% for **1**/Cy/TBHPorg) but also the ATR FT-IR spectrum of the recovered solid was identical to that for **1** (not shown).

Table 5. Catalytic Performance of Compounds 1−4 in the Epoxidation of *cis*-Cyclooctene at 55 °C

			epoxide yield at 6/24 h (%)	
catalyst	oxidant	solvent[a]	run 1	run 2
1	TBHPorg	nas	87/97	86/98
		$[BMIM]BF_4$	53/78	64/96
		$[BMpy]BF_4$	48/72	60/88
	dryTBHPorg	nas	100/100	
	TBHPaq	nas	49/72	
		$[BMIM]BF_4$	26/41	
		$[BMpy]BF_4$	22/39	
2	TBHPorg	nas	88/100	88/99
		$[BMIM]BF_4$	79/95	76/99
		$[BMpy]BF_4$	54/81	54/83
	TBHPaq	nas	48/72	
3	TBHPorg	nas	88/99	
4	TBHPorg	nas	46/76	
		$[BMIM]BF_4$	38/71	

[a] nas = no additional solvent.

In order to explore the versatility of complex **1**, similar catalytic tests (using olefin/dryTBHPorg reaction mixtures) were carried out for cyclic and linear olefins, namely, *R*-(+)-limonene, 1-octene, and *trans*-2-octene. Whereas *R*-(+)-limonene and *trans*-2-octene were completely converted at 6 h reaction, conversion of 1-octene was 21%. With the exception of limonene, the epoxide was always the only reaction product. In the case of limonene as substrate, selectivity to 1,2-epoxy-*p*-menthane and 1,2-8,9-diepoxy-*p*-menthane was 70% and 22%, respectively, and *p*-mentha-1,

dx.doi.org/10.1021/ic102456z |*Inorg. Chem.* 2011, 50, 3490–3500

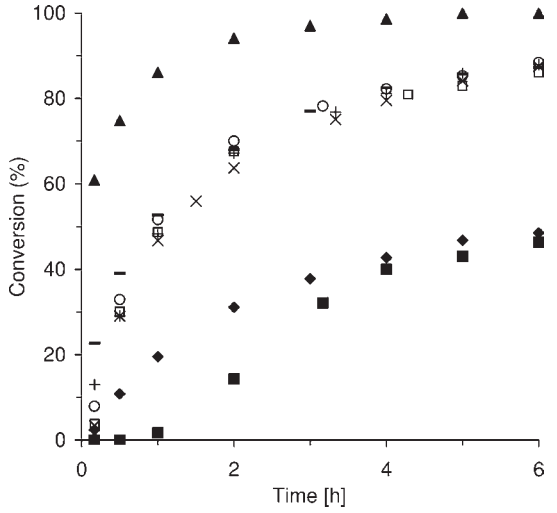

Figure 5. Epoxidation of *cis*-cyclooctene at 55 °C in the absence of cosolvent for **1** with TBHPorg [run 1 (—) and run 2 (□)], **1** with dryTBHPorg (▲), **1** with TBHPaq (♦), **2** with TBHPorg [run 1 (+) and run 2 (×)], **3** with TBHPorg (○), and **4** with TBHPorg (■).

8-dien-7-ol was formed with 8% selectivity at 100% conversion. These results further indicate regioselectivity toward the epoxidation of the endocyclic double bond relative to the exocyclic one. The higher reactivity of more nucleophilic substrates corroborates with the mechanism proposed for dioxomolybdenum(VI) complexes and alkylhydroperoxides as oxidants in that the higher electronic density of an olefinic double bond should favor the nucleophilic attack on an electrophilic oxidizing species formed from the reaction between the molybdenum complex and the oxidant.[24]

A further catalytic test for Cy epoxidation was carried out at 55 °C with complex **1** and 1,2-dichloroethane as cosolvent. Under these conditions (which, apart from the reaction temperature, are similar to those used to prepare **2** and **3**) the reaction mixture consisted of a yellow solid in suspension. The ATR FT-IR spectrum of the yellow solid recovered after the 24 h run was almost identical to that for the dinuclear complex **3**. Hence, formation of complex **3** in the catalytic system **1**/Cy/TBHPorg seems likely and would explain the presence (noted above) of free ligand in the liquid phase.

The catalytic performance of complex **1** for Cy epoxidation was subsequently examined using 70% aqueous TBHP (TBHPaq) as the oxidant instead of TBHPorg. The CyO yields at 6 and 24 h were much lower than those obtained with TBHPorg (CyO was always the only reaction product) (Table 5 and Figure 5). There are several possible reasons for these activity differences: (i) water may act as a coordinating solvent and inhibit the olefin reaction; (ii) the complex may be water sensitive; (iii) TBHP may be present in both phases of the liquid−liquid biphasic system, and mass transfer limitations may exist. The ATR FT-IR spectrum of the insoluble solid recovered after catalysis (**1**-TBHPaq) exhibited several notable differences (in the ranges of 750−1150 and 300−400 cm^{-1}) when compared with complex **1**, suggesting that the complex was not stable under the reaction conditions used (Figure S5 in the Supporting Information). Thus, the initially strong ν(Mo═O) band at 916 cm^{-1} was reduced to weak intensity, and new bands appeared at 898 (m) and 847 (s) cm^{-1}. In the region 1000−1100 cm^{-1} the broad ν(B−F) absorption centered around 1060 cm^{-1} for **1** was strongly reduced in the spectrum of **1**-TBHPaq, leaving only the fairly narrow ligand mode at 1041 cm^{-1}. Toward higher frequencies (1200−1600 cm^{-1}) no changes occurred with respect to the bands assigned to internal ligand modes. All of these differences were also evident (but to a lesser degree) in the ATR FT-IR spectrum of **1**-TBHPorg (Figure S5 in the Supporting Information). The absorption bands observed in the range of 300−1200 cm^{-1} in the ATR FT-IR spectrum of **4** (Figure S5 in the Supporting Information), which was prepared by the treatment of complex **1** with water, match the new bands described above for **1**-TBHPorg and **1**-TBHPaq, indicating that the changes observed in the spectra of the recovered solids (compared with **1**) are mainly due to the progressive formation of **4**, with the relative amount of this species increasing with the water content of the reaction mixture.

The solid **4** was tested in the Cy reaction with TBHPorg at 55 °C (Table 5 and Figure 5). An initial induction period of at least 30 min was observed, possibly due to the very poor solubility of the solid in the reaction medium, and the epoxide yields at 6/24 h (46%/76%) were much lower than those observed for **1** (87%/97%); CyO was always the only reaction product. The ATR FT-IR spectrum of the solid recovered after the 24 h run (Figure S6 in the Supporting Information) was identical to that for **4**, showing that the compound is stable under the reaction conditions used.

To completely dissolve complex **1** and TBHPorg, the ionic liquids (ILs) 1-butyl-3-methylimidazolium tetrafluoroborate ([BMIM]BF_4) and *N*-butyl-3-methylpyridinium tetrafluoroborate ([BMPy]BF_4) were used as solvents. The two ILs gave comparable catalytic results, suggesting that the cation of the IL has only a minor influence on the Cy reaction (Figure 6 and Table 5). CyO was always the only product, obtained in 48−53/72−78% yield at 6/24 h reaction. These results are on a par with those reported in the literature for [MoO_2Cl(L)]Y/IL catalytic systems: for L = $HC(bim)_3$,[9] 40−80% CyO yield at 24 h; for L = Bn_3Me_3-tame,[23] 60−79% CyO yield at 30 h, and the corresponding diol was formed as a byproduct in 11−14% yield. The metal complex/IL systems were recycled after centrifugation and extraction of CyO with *n*-hexane (which is immiscible with the IL and does not dissolve complex **1**); the complete extraction of Cy and CyO from the metal complex/IL system was confirmed by GC, and ICP-AES analyses indicated that no measurable amounts of molybdenum were extracted. The recovered catalyst/IL mixtures were recharged with olefin and TBHPorg, and the catalytic reactions were monitored for a further 24 h at 55 °C (Figure 6 and Table 5). For both recovered catalyst/IL mixtures, higher CyO yields were reached at 6/24 h in the second runs (88−96% at 24 h), possibly due to the accumulation of TBHP in the recycled complex/IL mixture, accounting for higher initial oxidant:olefin and oxidant:molybdenum molar ratios. Nevertheless, the efficiency in recovering the metal complex/IL mixtures without loss of metal is a major issue for the excellent catalytic performance observed.

As described in the synthesis section above, reaction of **1** in CH_2Cl_2 with a large excess (150 equiv) of the oxidant TBHP (5−6 M in decane) resulted in isolation of the dinuclear complexes **2** and **3**. The fact that species **4** was not isolated in these experiments may be because the reactions were carried out at room temperature with a solvent, while the catalytic reactions that gave solids containing **4** were carried out at 55 °C without a cosolvent, and reaction of **1** with water was carried out under reflux. The catalytic performance of **2** and **3** for reaction of Cy

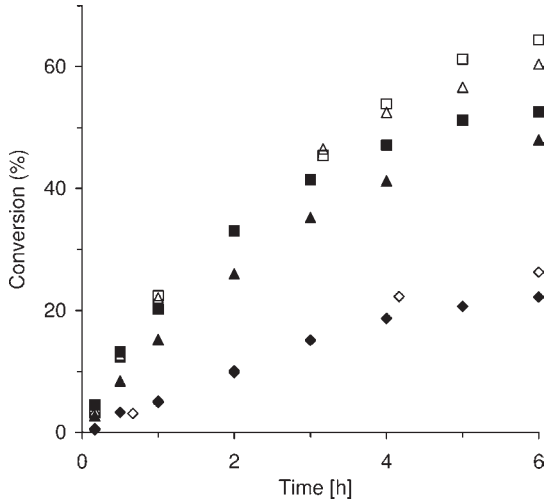

Figure 6. Epoxidation of *cis*-cyclooctene with TBHPorg or TBHPaq using an IL as cosolvent at 55 °C. For TBHPorg: **1**/[BMIM]BF_4 [run 1 (■) and run 2 (□)] and **1**/[BMPy]BF_4 [run 1 (▲) and run 2 (Δ)]. For TBHPaq: **1**/[BMIM]BF_4 (◇) and **1**/[BMPy]BF_4 (♦).

with TBHPorg was similar to that for **1**, with CyO being the only product formed in 88/100% yield at 6/24 h (Table 5). Only the initial reaction rates (based on conversions up to 1 h) were significantly different for the three complexes: conversion at 10 min decreased in the order **1** (23%) > **2** (13%) > **3** (8%). The reaction mixtures at 24 h consisted of a beige (for **2**) or yellow (for **3**) solid suspended in a yellow liquid. The solids were recovered (giving **2**-TBHPorg and **3**-TBHPorg), and **2**-TBHPorg was used in a second run, giving a kinetic curve that was essentially coincident with that for the first run. Unlike **1** and **1**-TBHPorg, the ATR FT-IR spectra of **2**-TBHPorg and **3**-TBHPorg were quite similar to those for **2** and **3**, respectively (Figure S6 in the Supporting Information), indicating that the dinuclear complexes are more stable than **1** under the reaction conditions used. Complexes **2** and **3** were treated with water as described above for **1**, giving the solids referred to as **2**-H_2O and **3**-H_2O. The IR spectrum of **2**-H_2O was identical to that for **4**, while the spectrum of **3**-H_2O was similar to that for **3** (Figure S5 in the Supporting Information).

For complex **2** reaction of Cy with TBHPorg was also carried out using the ILs [BMIM]BF_4 or [BMPy]BF_4 as solvent, which gave CyO yields at 24 h of 95% and 81%, respectively (Table 5). Both of the metal complex/IL systems could be recycled (as described above for **1**) and reused with no loss of catalytic performance (Table 5). A similar catalytic test performed for complex **4**/[BMIM]BF_4 gave 38/71% conversion at 6/24 h (selectivity to CyO was always 100%); complex **4** was insoluble in the IL (Table 5). The ATR FT-IR spectrum of the solid recovered from this reaction (not shown) was similar to that for **4**, suggesting that the complex is stable in the IL mixture. The slower epoxidation reactions for the systems with ILs in comparison to those without additional cosolvent may be partly due to mass transfer limitations.

CONCLUDING REMARKS

The mononuclear complex $[MoO_2Cl\{HC(3,5\text{-}Me_2pz)_3\}]BF_4$ (**1**) can be obtained in good yield by replacement of the coordinated solvent molecules in $[MoO_2Cl(THF)_3](BF_4)$ by the tris(3,5-dimethyl-1-pyrazolyl)methane) ligand. Recrystallization of **1** gave single crystals of the symmetrical dioxido(μ-oxido)molybdenum(VI) complex, $[Mo_2O_4(\mu_2\text{-}O)\{HC(3,5\text{-}Me_2pz)_3\}_2](BF_4)_2$ (**2**), rather than the mononuclear complex **1**, which is in agreement with several studies in the literature that indicate a tendency of Tpm−Mo mononuclear complexes to form dinuclear derivatives. When complex **1** is dissolved in dichloromethane and treated with excess TBHP at room temperature, the unusual unsymmetrical $[Mo_2O_3(O_2)_2(\mu_2\text{-}O)(H_2O)\{HC(3,5\text{-}Me_2pz)_3\}]$ (**3**) precipitates from the reaction mixture and complex **2** can be isolated from the liquid phase. When used as catalysts for the liquid-phase epoxidation of *cis*-cyclooctene with TBHP as the oxidant, complexes **1**−**3** exhibit comparable performance, giving epoxycyclooctane as the only product. Taking into account the conditions under which **2** and **3** were obtained (starting from **1**), these dinuclear complexes may be present in the **1**/Cy/TBHP system and contribute to the catalytic behavior. However, under the catalytic reaction conditions used, transformation of **1** into the less active compound **4** is significant, especially in the presence of water. Formation of **4** can be avoided and the catalytic activity maximized by rigorously drying the substrate/oxidant mixture prior to addition of the catalyst.

EXPERIMENTAL SECTION

Materials and Methods. Microanalyses for CHN were performed at the University of Aveiro. Quantification of molybdenum in the samples was performed at the University of Aveiro (Lina Carvalho, Eugénio Soares) by inductively coupled plasma optical emission spectroscopy (ICP-OES) after acid digestion of the sample (10% experimental error). Quantification of Cl was carried out using a Dionex 2000i/SP ion chromatography workstation with a conductivity detector (C. Patinha, University of Aveiro). An isocratic elution with a $NaHCO_3$−Na_2CO_3 solution was employed together with a Dionex AS4 anion separator column. Transmission IR spectra were recorded on a Mattson 7000 FT-IR spectrometer. Attenuated total reflectance (ATR) FT-IR spectra were measured on the same instrument equipped with a Specac Golden Gate Mk II ATR accessory having diamond top-plate and KRS-5 focusing lenses. FT-Raman spectra were recorded on a Bruker RFS 100 spectrometer with a Nd:YAG coherent laser (λ = 1064 nm). ^{1}H NMR spectra were acquired at room temperature using a Bruker CXP 300 spectrometer and referenced to TMS.

All air-sensitive preparations and manipulations were carried out using standard Schlenk techniques under nitrogen with solvents dried by standard procedures. The reagents 3,5-dimethylpyrazole (99%, Aldrich), K_2CO_3 (Riedel de Häen), tetrabutylammonium hydrogen sulfate (97%, Sigma-Aldrich), and MoO_2Cl_2 (Aldrich) were purchased from commercial sources and used as received. Thallium tetrafluoroborate was prepared from Tl_2CO_3 and HBF_4 in water and vacuum dried at 80 °C prior to use. The TBHP solution (5.0−6.0 M in decane, containing up to 4% water) was used as received.

Tris(3,5-dimethyl-1-pyrazolyl)methane [$HC(3,5\text{-}Me_2pz)_3$]. The ligand $HC(3,5\text{-}Me_2pz)_3$ was prepared as described in the literature with minor changes.[3a] A mixture of dimethylpyrazole (11.54 g, 0.12 mol), anhydrous K_2CO_3 (82.93 g, 0.60 mol), and $(Bu_4N)HSO_4$ (2.04 g, 6 mmol) was stirred and refluxed in $CHCl_3$ (100 mL) for 19 h. The resultant dark brown mixture was filtered, and the solid was washed with hot CH_2Cl_2. The organic solution was evaporated to dryness, and the crude product was purified by column chromatography (silica) using diethyl ether/hexane (1:1) as eluent. After concentrating the yellow solution, it was stored in a fridge overnight and the resultant precipitate was filtered and washed with pentane. Yield: 4.0 g, 34%. Anal. Calcd for $C_{16}H_{22}N_6$ (298.39): C, 64.40; H, 7.43; N, 28.16. Found: C, 64.22; H,

dx.doi.org/10.1021/ic102456z |*Inorg. Chem.* 2011, 50, 3490–3500

Table 6. Crystal and Structure Refinement Data for Compounds $[Mo_2O_4(\mu_2\text{-}O)\{HC(3,5\text{-}Me_2pz)_3\}_2](BF_4)_2$ (2) and $[Mo_2O_3(O_2)_2(\mu_2\text{-}O)(H_2O)\{HC(3,5\text{-}Me_2pz)_3\}]\cdot 3H_2O$ (3)

	2 (SQUEEZE)	3
formula	$C_{32}H_{44}B_2F_8Mo_2N_{12}O_5$	$C_{16}H_{30}N_6O_{12}Mo_2$
M_r [g mol^{-1}]	1042.26	690.32
crystal description	colorless blocks	yellow plates
crystal size [mm]	0.14 × 0.12 × 0.12	0.20 × 0.16 × 0.06
T [K]	150(2)	180(2)
cryst syst	triclinic	monoclinic
space group	$P\bar{1}$	$P2_1/c$
a [Å]	17.9727(5)	12.7169(6)
b [Å]	18.8894(5)	15.6739(8)
c [Å]	23.4086(7)	13.9182(7)
α [deg]	73.354(2)	
β [deg]	75.827(2)	115.405(2)
γ [deg]	68.6830(10)	
V [Å^3]	7004.4(3)	2505.9(2)
Z	6	4
ρ_{calcd} [g cm^{-3}]	1.483	1.830
$F(000)$	3156	1392
μ [mm^{-1}]	0.618	1.071
θ range [deg]	3.55−25.35	3.55−29.13
index ranges	$-21 \le h \le 21$	$-17 \le h \le 17$
	$-22 \le k \le 22$	$-21 \le k \le 21$
	$-28 \le l \le 25$	$-19 \le l \le 18$
no. of reflns collected	190 551	66 423
no. of independent reflns	25 019 (R_{int} = 0.0769)	6731 (R_{int} = 0.0357)
final R indices $[I > 2\sigma(I)]^a$	R_1 = 0.0836	R_1 = 0.0247
	wR_2 = 0.2531	wR_2 = 0.0508
final R indices (all data)^a	R_1 = 0.1122	R_1 = 0.0408
	wR_2 = 0.2712	wR_2 = 0.0572
largest diff peak and hole [eÅ^{-3}]	3.774 and −2.835	0.461 and −0.823

$^a R_1 = \Sigma||F_o| - |F_c||/\Sigma|F_o|$. $wR_2 = (\Sigma[w(F_o^2 - F_c^2)^2]/\Sigma[w(F_o^2)])^{1/2}$.

7.50; N, 28.68. Selected IR (KBr, cm^{-1}): 3131 (m), 3039 (m), 2984 (s), 2956 (s), 2924 (s), 2869 (m), 1562 (vs), 1471 (s), 1449 (s), 1414 (s), 1376 (s), 1347 (s), 1320 (s), 1274 (s), 1252 (s), 1139 (s), 1031 (s), 986 (m), 971 (m), 881 (m), 862 (s), 827 (s), 778 (s), 762 (m), 709 (m), 699 (s), 624 (s). Selected Raman (cm^{-1}): 3128, 3096, 2985, 2957, 2925, 2875, 2747, 1561, 1450, 1388, 1026, 591, 217, 194. ^{1}H NMR (300 MHz, DMSO-d_6): δ (ppm) = 8.30 (s, 1H, CH), 5.94 (s, 3H, H-4), 2.06 (s, 9H, CH_3 in position 3), 1.94 (s, 9H, CH_3 in position 5).

$[MoO_2Cl\{HC(3,5\text{-}Me_2pz)_3\}]BF_4$ (1). One equivalent of $TlBF_4$ was added to a solution of MoO_2Cl_2 (0.50 g, 2.51 mmol) in THF (15 mL), resulting in the immediate precipitation of colorless TlCl. After stirring the mixture for 15 min the pale yellow solution was filtered off and treated with $HC(3,5\text{-}Me_2pz)_3$ (0.75 g, 2.51 mmol). An off-white precipitate formed, and the mixture was stirred for 1 h at room temperature. After evaporating the solvent under reduced pressure, the solid was washed three times with diethyl ether and vacuum dried. Yield: 0.90 g, 65%. Anal. Calcd for $C_{16}H_{22}BClF_4MoN_6O_2$ (548.58): C, 35.03; H, 4.04; N, 15.32; Cl, 6.46. Found: C, 35.51; H, 4.68; N, 15.00; Cl, 6.98. Selected IR (KBr, cm^{-1}): 3139 (m), 3015 (m), 2975 (m), 2932 (m), 2871 (m), 1563 (vs), 1459 (s), 1415 (s), 1377 (s), 1303 (s), 1259 (s), 1124 (m), 1082 (sh), 1060 (vs), 1047 (s), 987 (sh), 951 (s), 916 (vs), 857 (m), 837 (m), 806 (m), 762 (s), 708 (s), 519 (s), 490 (s), 399 (m), 378 (m), 361 (s), 314 (m). Selected Raman (cm^{-1}): 3140, 3015, 2933, 1562, 1461, 1382, 1299, 1160, 1123, 1063, 1048, 1018, 952, 944, 918, 763, 597, 492, 483, 411, 401, 361, 282, 248, 208. ^{1}H NMR (300 MHz, DMSO-d_6): δ (ppm) = 8.30 (s, 1H, CH), 5.94 (s, 3H, H-4), 2.06 (s, 9H, CH_3 in position 3), 1.94 (s, 9H, CH_3 in position 5).

$[Mo_2O_4(\mu_2\text{-}O)\{HC(3,5\text{-}Me_2pz)_3\}_2](BF_4)_2$ (2). A large excess (ca. 150 equiv.) of TBHP (5.0−6.0 M in decane) was added to a solution of **1** (140 mg, 0.26 mmol) in CH_2Cl_2 (15 mL). The resultant yellow solution was stirred for 24 h at room temperature, during which time a yellow solid precipitated. The mixture was filtered, and MnO_2 was added to the filtrate to destroy the excess peroxide. After filtering off the solution it was concentrated and mixed with diethyl ether. The colorless solid that precipitated was filtered, washed with diethyl ether and *n*-pentane, and vacuum dried. Yield: 0.04 g, 30%. Anal. Calcd for $C_{32}H_{44}B_2F_8Mo_2N_{12}O_5$ (1042.26): C, 36.88; H, 4.26; N, 16.13. Found: C, 36.65; H, 4.60; N, 16.07. IR (KBr, cm^{-1}): 3129 (w), 2980 (sh), 2896 (w), 2778 (w), 2666 (w), 1562 (vs), 1459 (s), 1415 (m), 1379 (vs), 1303 (s), 1263 (s), 1071 (sh), 1046 (vs), 993 (w), 945 (s), 916 (vs), 859 (s), 766 (vs), 704 (m), 630 (m), 533 (m), 521 (m), 490 (m), 484 (sh), 394 (s), 323 (s). ^{1}H NMR (300 MHz, DMSO-d_6): δ (ppm) = 8.31 (s, 2H, CH), 5.95 (s, 6H, H-4), 2.07 (s, 18H, CH_3 in position 3), 1.95 (s, 18H, CH_3 in position 5).

$[Mo_2O_3(O_2)_2(\mu_2\text{-}O)(H_2O)\{HC(3,5\text{-}Me_2pz)_3\}]\cdot 3H_2O$ (3). The yellow precipitate obtained in the above procedure was washed with diethyl ether, vacuum dried, and recrystallized from 1,2-dichloroethane/diethyl ether/pentane. Yield: 0.024 g, 27%. Anal. Calcd for $C_{16}H_{30}Mo_2N_6O_{12}$ (690.32): C, 27.84; H, 4.38; N, 12.17. Found: C, 28.08; H, 3.55; N, 12.12. IR (KBr, cm^{-1}): 3139 (w), 3068 (sh), 2976 (w), 2921 (w), 2848 (sh), 1564 (s), 1460 (s), 1414 (m), 1380 (w), 1302 (s), 1266 (s), 1156 (sh), 1121 (w), 1083 (w), 1046 (s), 985 (m), 954 (vs), 915 (s), 862 (m), 794 (m), 760 (m), 702 (w), 629 (w), 567 (w), 489 (w), 434 (w), 394 (w), 354 (w), 320 (m). Raman (cm^{-1}): 3142, 2929, 1463, 1382, 1304, 986, 948, 920, 597, 286, 205. ^{1}H NMR (300 MHz, DMSO-d_6): δ (ppm) = 8.31 (s, 1H, CH), 5.95 (s, 3H, H-4), 2.08 (s, 9H, CH_3 in position 3), 1.95 (s, 9H, CH_3 in position 5).

$[\{HC(3,5\text{-}Me_2pz)_3\}MoO_3]$ (4). A suspension of **1** (0.85 g, 1.55 mmol) in water (40 mL) was refluxed for 2 h. A white precipitate was obtained, which was washed with water, acetone, and pentane and vacuum dried. Yield: 0.35 g, 51%. Anal. Calcd for $C_{16}H_{22}MoN_6O_3$ (442.32): C, 43.45; H, 5.01; N, 19.00; Mo, 21.69. Found: C, 43.58; H, 5.05; N, 18.84; Mo, 22.20. IR (KBr, cm^{-1}): 3133 (m), 3103 (m), 2999 (w), 2987 (w), 2956 (m), 2921 (m), 1565 (vs), 1461 (s), 1409 (m), 1385 (s), 1304 (vs), 1260 (vs), 1115 (s), 1042 (vs), 992 (s), 899 (vs), 861 (vs), 840 (sh), 781 (s), 703 (vs), 667 (m), 631 (m), 602 (m), 490 (m), 384 (s), 366 (m), 350 (m), 328 (w), 275 (m). Raman (cm^{-1}): 3135, 2987, 2919, 1566, 1465, 1391, 1057, 898, 862, 849, 603, 351, 242.

Single-Crystal X-ray Diffraction. Crystallographic data collection and structure refinement details are summarized in Table 6. Single crystals of $[Mo_2O_4(\mu_2\text{-}O)\{HC(3,5\text{-}Me_2pz)_3\}_2](BF_4)_2$ (**2**) and $[Mo_2O_3(O_2)_2(\mu_2\text{-}O)(H_2O)\{HC(3,5\text{-}Me_2pz)_3\}]\cdot 3H_2O$ (**3**) were harvested from the crystallization vials and immediately immersed in highly viscous FOMBLIN Y perfluoropolyether vacuum oil (LVAC 140/13, Sigma-Aldrich) to avoid degradation caused by evaporation of the solvent. The crystals were mounted on a Hampton Research CryoLoop with the help of a Stemi 2000 stereomicroscope equipped with Carl Zeiss lenses.[25] Data were collected on a Bruker X8 Kappa APEX II CCD area-detector diffractometer (Mo $K\alpha$ graphite-monochromated radiation, λ = 0.71073 Å) controlled by the APEX2 software package[26] and equipped with an Oxford Cryosystems Series 700 cryostream monitored

remotely using the software interface Cryopad.[27] Images were processed using the software package SAINT+,[28] and data were corrected for absorption by the multiscan semiempirical method implemented in SADABS.[29] While the structure of **2** was solved using the Patterson synthesis algorithm implemented in SHELXS-97,[30] allowing the immediate location of the Mo centers, that of **3** was instead solved by direct methods using SHELXS-97,[30] permitting the direct location of the majority of the heaviest atoms. For the two structures all remaining non-hydrogen atoms were located from difference Fourier maps calculated from successive full-matrix least-squares refinement cycles on F^2 using SHELXL-97.[30a,31] All non-hydrogen atoms were successfully refined using anisotropic displacement parameters with the exception of the six crystallographically independent BF_4^- anions in **2**.

For the two structures H atoms bound to carbon were located at their idealized positions using appropriate *HFIX* instructions in SHELXL: 43 for the aromatic, 13 for the tertiary carbons, and 137 for the terminal $-CH_3$ methyl groups belonging to the $HC(3,5\text{-}Me_2pz)_3$ ligands. All these atoms were included in subsequent refinement cycles in riding-motion approximation with isotropic thermal displacements parameters (U_{iso}) fixed at 1.2 (aromatic and tertiary) or 1.5 ($-CH_3$ groups) times U_{eq} of the attached carbon atom. In **3** the hydrogen atoms associated with water molecules (coordinated and uncoordinated) were markedly visible in the difference Fourier maps and included in the final structure model during subsequent refinement stages with the O−H and H···H distances restrained to 0.95(1) and 1.55(1) Å, respectively. This procedure ensures a chemically reasonable geometry for these molecules. Atoms were treated using a riding-motion approximation with U_{iso} fixed at $1.5U_{eq}$ of the parent oxygen atom.

In **2** a total of six crystallographically independent BF_4^- anions were directly located in difference Fourier maps and included in the structural model with full site occupancy and rigid geometric constraints (B−F and F···F tetrahedral distances constrained to common refineable values) in order to ensure chemically reasonable environments for these moieties. This structure contains inner voids [the largest centered at (1/2 0 1/2), which most likely contain highly disordered solvent molecules (diethyl ether and *n*-pentane). Attempts to locate and model these solvent molecules were unfruitful due to the considerable smeared-out electron density located inside the cavities. In addition, the lack of well-defined electron density peaks further promoted unstable structural refinements even when rigid geometric constraints were employed for the included solvent moieties. The structural reliability factors converged, at this stage, to $R1$ [$I > 2\sigma(I)$] = 0.1471 and $wR2$ (all data) = 0.2886. PLATON[32] estimated that the residual solvent-accessible volume encloses about 1093 Å^3 (ca. 15.6% of the total volume of the unit cell); see Figure S3 in the Supporting Information. The original data set was mathematically treated using SQUEEZE[33] in order to remove the contribution of these highly disordered molecules. It was ultimately estimated that the aforementioned cavities would contain ca. 527 electrons. The calculated solvent-free reflection list was used for further structural refinements, which converged to the solvent-free structure reported in this manuscript having the reliability factors summarized in Table 6.

The oxidation states of the molybdenum centers in **2** were further investigated using PLATON,[32] following closely the theoretical models of Brese and O'Keeffe[34] and Brown and Altermatt.[35] The sums of the bond valences at each atomic position are as follows (considering a +6 oxidation state for each metal center): Mo(1) +6.26; Mo(2) +6.09; Mo(3) +6.18; Mo(4) +6.10; Mo(5) +6.00; Mo(6) +6.09.

The last difference Fourier map synthesis showed the following: for **2**, the highest peak (3.774 eÅ^{-3}) and deepest hole (−2.835 eÅ^{-3}) located at 0.07 and 0.12 Å from F(1) and F(20), respectively; for **3**, the highest peak (0.461 eÅ^{-3}) and deepest hole (−0.823 eÅ^{-3}) located at 0.72 and 0.66 Å from C(6) and Mo(2), respectively. CCDC-764428 (**2**) and CCDC-771365 (**3**) contain the supplementary crystallographic data for this paper (excluding structure factors). These data can be obtained free of charge from The Cambridge Crystallographic Data Centre via www.ccdc.cam.ac.uk/data_request/cif.

Catalysis. The liquid-phase epoxidation of *cis*-cyclooctene (Cy) was carried out at atmospheric pressure in borosilicate microreactors equipped with a magnetic stirrer and a valve for sampling. Typically, the reactors were loaded with the metal complex (in an amount equivalent to 16 μmol of molybdenum), 1.6 mmol of Cy, and 2.75 mmol of oxidant, and immersed in a thermostatted oil bath at 55 °C (this instant is taken as time zero). The oxidants used were 5.0−6.0 M *tert*-butylhydroperoxide in decane, which contains up to 4% water (denoted TBHPorg), and 70% aqueous TBHP (TBHPaq). The reactions were carried out without adding a cosolvent or using 1,2-dichloroethane (2 mL) or an ionic liquid, 1-butyl-3-methylimidazolium tetrafluoroborate ($[BMIM]BF_4$) or *N*-butyl-3-methylpyridinium tetrafluoroborate ($[BMPy]BF_4$) (100 μL), as cosolvent. For some catalytic tests water was removed from the Cy/TBHP solution using 4 Å molecular sieves that had been previously activated by heating at 180 °C under vacuum for 16 h; after the molecular sieves were separated from the Cy/TBHP solution, the metal complex was added and the reaction mixture was immersed in the thermostatted oil bath. After a 24 h-run the solid and liquid phases were separated via centrifugation and filtration (0.2 μm Cronus PTFE membrane). The solid was thoroughly washed with *n*-pentane and dried at room temperature overnight prior to characterization/reuse. Catalytic reactions were monitored by gas chromatography (V3900 GC-FID) using a capillary column (DB-5, 30 m × 0.25 mm).

■ ASSOCIATED CONTENT

Supporting Information. Crystallographic data for compounds **2** and **3** in CIF format, representations of the asymmetric units of **2** and **3**, crystal packing of **2**, unaccounted solvent-accessible area in the crystal structure model of **2**, details of the Le Bail whole-powder-diffraction-pattern profile fitting for **4**, and ATR FT-IR spectra. This material is available free of charge via the Internet at http://pubs.acs.org.

■ AUTHOR INFORMATION

Corresponding Author

* E-mail: atav@ua.pt (A.A.V.); igoncalves@ua.pt (I.S.G.).

■ ACKNOWLEDGMENT

We are grateful to the Fundação para a Ciência e a Tecnologia (FCT), the Programa Operacional "Ciência e Inovação 2010" (POCI 2010), the Orçamento do Estado (OE), and the Fundo Europeu de Desenvolvimento Regional (FEDER) for funding through the projects PTDC/QUI/71198/2006 and PTDC/QUI/65805/2006. P.N., S.S.B., and S.G. thank the FCT for grants. We are also grateful to the FCT for financial support toward the purchase of the single-crystal diffractometer.

■ REFERENCES

(1) (a) Bigmore, H. R.; Lawrence, S. C.; Mountford, P.; Tredget, C. S. *Dalton Trans.* **2005**, 635–651. (b) Pettinari, C.; Pettinari, R. *Coord. Chem. Rev.* **2005**, *249*, 525–543.

(2) Trofimenko, S. *J. Am. Chem. Soc.* **1970**, *92*, 5118–5126.

(3) (a) Julia, S.; del Mazo, J. M.; Avila, L.; Elguero, J. *Org. Prep. Proc. Int.* **1984**, *16*, 299–307. (b) Reger, D. L.; Grattan, T. C.; Brown, K. J.; Little, C. A.; Lamba, J. J. S.; Rheingold, A. L.; Sommer, R. D.

J. Organomet. Chem. **2000**, *607*, 120–128. (c) Goodman, M. S.; Bateman, M. A. *Tetrahedron Lett.* **2001**, *42*, 5–7.

(4) (a) Reger, D. L. *Comments Inorg. Chem.* **1999**, *21*, 1–28. (b) Garcia, R.; Paulo, A.; Santos, I. *Inorg. Chim. Acta* **2009**, *362*, 4315–4327.

(5) Dilsky, S. *J. Organomet. Chem.* **2007**, *692*, 2887–2896.

(6) Dhawan, I. K.; Bruck, M. A.; Schilling, B.; Grittini, C.; Enemark, J. H. *Inorg. Chem.* **1995**, *34*, 3801–3808.

(7) Dinoi, C.; da Silva, M. F. C. G.; Alegria, E. C. B. A.; Smoleński, P.; Martins, L. M. D. R. S.; Poli, R.; Pombeiro, A. J. L. *Eur. J. Inorg. Chem.* **2010**, 2415–2424.

(8) Santos, A. M.; Kühn, F. E.; Bruus-Jensen, K.; Lucas, I.; Romão, C. C.; Herdtweck, E. *J. Chem. Soc., Dalton Trans.* **2001**, 1332–1337.

(9) Gago, S.; Balula, S. S.; Figueiredo, S.; Lopes, A. D.; Valente, A. A.; Pillinger, M.; Gonçalves, I. S. *Appl. Catal. A: Gen.* **2010**, *372*, 67–72.

(10) (a) Arzoumanian, H.; Bakhtchadjian, R.; Agrifoglio, G.; Atencio, R.; Briceño, A. *Transition Met. Chem.* **2006**, *31*, 681–689. (b) Pereira, C. C. L.; Balula, S. S.; Paz, F. A. A.; Valente, A. A.; Pillinger, M.; Klinowski, J.; Gonçalves, I. S. *Inorg. Chem.* **2007**, *46*, 8508–8510. (c) Gago, S.; Neves, P.; Monteiro, B.; Pessêgo, M.; Lopes, A. D.; Valente, A. A.; Paz, F. A. A.; Pillinger, M.; Moreira, J.; Silva, C. M.; Gonçalves, I. S. *Eur. J. Inorg. Chem.* **2009**, 4528–4537.

(11) (a) Djordjevic, C.; Gundersen, J. L.; Jacobs, B. A.; Sinn, E. *Polyhedron* **1989**, *8*, 541–543. (b) Grzywa, M.; Nitek, W.; Lasocha, W. *J. Mol. Struct.* **2008**, *888*, 318–326. (c) Le Carpentier, J.-M.; Mitschler, A.; Weiss, R. *Acta Crystallogr., Sect. B: Struct. Sci.* **1972**, *28*, 1288–1298.

(12) Bernstein, J.; Davis, R. E.; Shimoni, L.; Chang, N. L. *Angew. Chem., Int. Ed.* **1995**, *34*, 1555–1573.

(13) Lakshminarayanan, P. S.; Kumar, D. K.; Ghosh, P. *Inorg. Chem.* **2005**, *44*, 7540–7546.

(14) Zhu, W. H.; Wang, Z. M.; Gao, S. *Dalton Trans.* **2006**, 765–768.

(15) Prasad, T. K.; Rajasekharan, M. V. *Cryst. Growth Des.* **2006**, *6*, 488–491.

(16) Barbour, L. J.; Orr, G. W.; Atwood, J. L. *Nature* **1998**, *393*, 671–673.

(17) Neogi, S.; Savitha, G.; Bharadwaj, P. K. *Inorg. Chem.* **2004**, *43*, 3771–3773.

(18) (a) Ghosh, S. K.; Bharadwaj, P. K. *Inorg. Chem.* **2004**, *43*, 6887–6889. (b) Soares-Santos, P. C. R.; Cunha-Silva, L.; Paz, F. A. A.; Ferreira, R. A. S.; Rocha, J.; Carlos, L. D.; Nogueira, H. I. S. *Inorg. Chem.* **2010**, *49*, 3428–3440. (c) Cunha-Silva, L.; Mafra, L.; Ananias, D.; Carlos, L. D.; Rocha, J.; Paz, F. A. A. *Chem. Mater.* **2007**, *19*, 3527–3538.

(19) Reger, D. L.; Semeniuc, R. F.; Pettinari, C.; Luna-Giles, F.; Smith, M. D. *Cryst. Growth Des.* **2006**, *6*, 1068–1070.

(20) Shi, F. N.; Cunha-Silva, L.; Ferreira, R. A. S.; Mafra, L.; Trindade, T.; Carlos, L. D.; Paz, F. A. A.; Rocha, J. *J. Am. Chem. Soc.* **2008**, *130*, 150–167.

(21) (a) Huang, Y. G.; Gong, Y. Q.; Jiang, F. L.; Yuan, D. Q.; Wu, M. Y.; Gao, Q.; Wei, W.; Hong, M. C. *Cryst. Growth Des.* **2007**, *7*, 1385–1387. (b) Kristiansson, O. *Eur. J. Inorg. Chem.* **2002**, 2355–2361. (c) Rocha, J.; Shi, F. N.; Paz, F. A. A.; Mafra, L.; Sardo, M.; Cunha-Silva, L.; Chisholm, J.; Ribeiro-Claro, P.; Trindade, T. *Chem.—Eur. J.* **2010**, *16*, 7741–7749.

(22) (a) Ludwig, R. *Angew. Chem., Int. Ed.* **2001**, *40*, 1808–1827. (b) Mascal, M.; Infantes, L.; Chisholm, J. *Angew. Chem., Int. Ed.* **2006**, *45*, 32–36.

(23) Petrovski, Z.; Valente, A. A.; Pillinger, M.; Dias, A. S.; Rodrigues, S. S.; Romão, C. C.; Gonçalves, I. S. *J. Mol. Catal. A: Chem.* **2006**, *249*, 166–171.

(24) (a) Kühn, F. E.; Groarke, M.; Bencze, E.; Herdtweck, E.; Prazeres, A.; Santos, A. M.; Calhorda, M. J.; Romão, C. C.; Gonçalves, I. S.; Lopes, A. D.; Pillinger, M. *Chem.—Eur. J.* **2002**, *8*, 2370–2381. (b) Veiros, L. F.; Prazeres, Â.; Costa, P. J.; Romão, C. C.; Kühn, F. E.; Calhorda, M. J. *Dalton Trans* **2006**, 1383–1389. (c) Mitchell, J. M.; Finney, N. S. *J. Am. Chem. Soc.* **2001**, *123*, 862–869. (d) Groarke, M.; Gonçalves, I. S.; Herrmann, W. A.; Kühn, F. E. *J. Organomet. Chem.* **2002**, *649*, 108–112.

(25) Kottke, T.; Stalke, D. *J. Appl. Crystallogr.* **1993**, *26*, 615–619.

(26) *APEX2, Data Collection Software*, version 2.1-RC13; Bruker AXS: Delft, The Netherlands, 2006.

(27) *Cryopad, Remote monitoring and control*, version 1.451; Oxford Cryosystems: Oxford, U.K., 2006.

(28) *SAINT+, Data Integration Engine*, version 7.23a; Bruker AXS: Madison, WI, 2005.

(29) Sheldrick, G. M. *SADABS, Bruker/Siemens Area Detector Absorption Correction Program*, version 2.01; Bruker AXS: Madison, WI, 1998.

(30) (a) Sheldrick, G. M. *Acta Crystallogr., Sect. A: Found. Crystallogr.* **2008**, *64*, 112–122. (b) Sheldrick, G. M. *SHELXS-97, Program for Crystal Structure Solution*; University of Göttingen: Göttingen, Germany, 1997.

(31) Sheldrick, G. M. *SHELXL-97, Program for Crystal Structure Refinement*; University of Göttingen: Göttingen, Germany, 1997.

(32) (a) Spek, A. L. *Acta Crystallogr., Sect. A: Found. Crystallogr.* **1990**, *46*, C34. (b) Spek, A. L. *J. Appl. Crystallogr.* **2003**, *36*, 7–13.

(33) Van der Sluis, P.; Spek, A. L. *Acta Crystallogr., Sect. A: Found. Crystallogr.* **1990**, *46*, 194–201.

(34) Brese, N. E.; O'Keeffe, M. *Acta Crystallogr., Sect. B: Struct. Sci.* **1991**, *47*, 192–197.

(35) Brown, I. D.; Altermatt, D. *Acta Crystallogr., Sect. B: Struct. Sci.* **1985**, *41*, 244–247.